New Approaches for Iris Boundary Localization

Dídac Pérez[1], Carles Fernández[1], Carlos Segura[1], Javier Hernando[2]

[1]Herta Security, S.L.,
[2]Theory of Signal and Communications, Universitat Politècnica de Catalunya
Barcelona, Spain
didac.perez@hertasecurity.com

Abstract. Iris segmentation is the most determining factor in iris biometrics, which has traditionally assumed rigid constrained environments. In this work, a novel method that covers the localization of the pupillaty and limbic iris boundaries is proposed. The algorithm consists of an energy minimization procedure posed as a multilabel one-directional graph and the use of physiological priors, achieving accurate segmentations even in the presence of clutter, lenses, glasses, motion blur, and variable illumination. The contributions of this paper are a fast and reliable method for the accurate localization of the iris boundaries in low-constrained conditions, which has been evaluated over two public databases, and a new database for iris segmentation incorporating challenging iris images, which has been publicly released to the research community.

Keywords: image processing, iris biometrics, iris recognition

1 Introduction

An ideal biometric system using iris recognition would be desirably non-invasive for the users. Furthermore, new iris scanners provide on-the-move and at-a-distance technologies, capture samples in real-time, and operate in variable illumination conditions and in an entirely unsupervised manner. There is no acknowledged relationship between the unique patterns of the random iris and genetic factors excepts its pigmentation [12], which determines the color of the iris. In addition, the iris patterns of identical twins are uncorrelated, as well as the two irides of different persons. Nowadays, iris recognition systems have become a good topic of research due to the mentioned characteristics of iris biometrics in terms of security, robustness, and effectiveness.

Thus, when dealing with real, unconstrained scenarios, the obtained iris images tend to suffer from clutter, defocus, motion blur, corneal reflections, highlights and shadows, non-frontal views, and corruptions and occlusions the iris zone, such as eyelids, eyelashes, contact lenses, or glasses. This large number of problems motivates developing sophisticated segmentation stages that determine valid regions within the captured image. Iris isolation and extraction directly influences the accuracy of the final recognition process.

This paper is structured as follows: Section 2 explores the existing literature on iris segmentation. Section 3 describes the proposed methodology for rough pupil detection (3.2) and localization of the pupillary (3.3) and limbic (3.4) boundaries via graph cuts. The experimental evaluation of these techniques is provided in Section 4, and some final conclusions are drawn in Section 5.

2 Related work

Most of the literature on iris recognition bases its core segmentation on the techniques proposed by either Daugman [3] or Wildes [12]. Daugman's integro-differential operator searches over the image domain for the maximum in the blurred partial derivative, with respect to increasing radius r, of the normalized contour integral of $I(x, y)$ along a circular arc ds of radius r and center coordinates (x_0, y_0). In Eq. (1), $G_\sigma(r)$ is a smoothing function such as a Gaussian of scale σ. The complete operator searches iteratively for a maximum contour integral derivative with increasing radius at successively finer scales of analysis through the three parameter space of center coordinates and radius (r, x_0, y_0) defining the path of contour integration.

$$max_{(r,x_0,y_0)} \left| G_\sigma(r) * \frac{\partial}{\partial r} \oint_{r,x_0,y_0} \frac{I(x,y)}{2\pi r} ds \right| \tag{1}$$

On the other hand, the circular Hough transform is proposed by Wildes to estimate these boundaries by again detecting circular structures within the binary edge map of points $(x_j, y_j), j = 1, ..., n$, computed over the image gradient. The goal is to find the triplet of two-dimensional origin coordinates and radii that maximizes the expression $H(x_c, y_c, r)$ in Eq. (2):

$$H(x_c, y_c, r) = \sum_{j=1}^{n} h(x_j, y_j, x_c, y_c, r) \tag{2}$$

where $h(x_j, y_j, x_c, y_c, r) = 1$ when $(x_j - x_c)^2 + (y_j - y_c)^2 - r^2 = 0$.

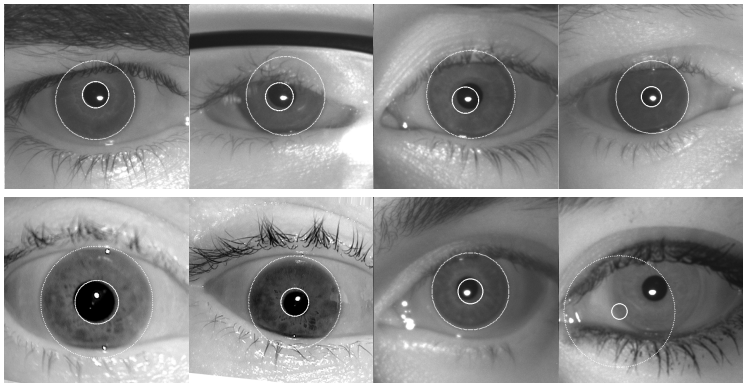

Fig. 1. Some examples of failure or non-exact segmentations using the methods proposed by Daugman —top row— and Wildes —bottom row—. Sample images from HID and ND-IRIS-0405 databases.

The abovementioned methods and their derivations [7, 10] present problems such as the exhaustive searches and the computation of edge maps, which is an unresolved

problem of computer vision. Hence, techniques based on elastic models and active contours have also been very actively used [11, 6]. Such techniques present limitations, such as extreme sensitivity to initialization and parameter tuning, slow convergence rates, and falling into local minima produced by noise or background clutter. Most of the currently available methods combine the aforementioned strategies; for instance, [7] fuses two different algorithms, and in one of them the limbic boundaries are localized by a repeated process of Canny edge detection and Hough transform, ended with the application of an integro-differential operator. Some failures of the Daugman and Wildes algorithms are shown in Fig. 1.

3 Proposed methodology

In this work, a method which covers the first stages of the iris segmentation process is proposed, namely removal of specular reflections, coarse localization of the pupil, and precise segmentation of the pupillary and limbic iris boundaries, as can be seen in Fig. 2.

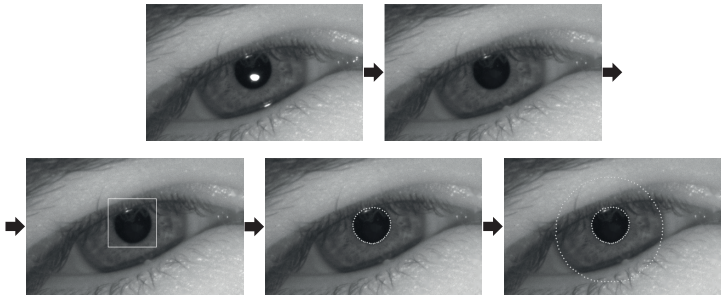

Fig. 2. Pipeline of the proposed methodology. From top left to down right: original image, removal of specular reflection, pupil localization, pupillary boundary localization, and limbic boundary localization. Sample captures from the HID dataset.

3.1 Removal of specularities

In our sequential approach the specular reflection removal is accomplished as a first step, since removing reflections becomes fundamental for coarse pupil localization and subsequent boundary localization, in the challenging cases in which the reflection invades the boundaries.

Our approach is inspired on the region-shrinking technique described in [9], with the difference that, instead of presetting a thresholding value, a modal analysis is carried out on the histogram of intensities to obtain a binary mask of highlights. Pixels in the binary mask are considered non-valid, and those having valid neighbors are given intensity values that are linearly interpolated from these neighbors. These pixels are removed from the list, and the process is repeated until all pixels are valid.

Fig. 3. Removal of specularity reflections from sample *04214d160* (ND-IRIS-0405 dataset).

3.2 Coarse localization of the pupil

First, candidate points are detected in a similar way to that proposed in [2], but again carrying out a modal analysis of the histogram to automatically compute an adaptive threshold above which the candidates are discarded.

The locations k of the remaining candidates in image I are scanned at different scales by a morphological filter H at different scales, which is computed by removing specular reflections from 200 annotated images from different datasets and averaging the aligned results. The estimated origin and radius of the pupil are those minimizing the test function appearing in Eq. (3).

$$\underset{x,y}{\operatorname{argmin}} \left| I(x,y) - H(x,y) \right|^2 \tag{3}$$

3.3 Pupillary boundary localization

Having estimated the pupil origin and size, the pupillary iris boundary is precisely localized using a method based on graph cuts, as can be seen in Fig. 4. The localization of iris boundaries can be posed as a multilabel energy minimization problem, and solved efficiently using graph cuts [1]. Let us consider the polar image of an eye centered at the estimated pupillary origin. We aim at finding the minimal cuts that separate the iris from the pupil and from the sclera, which would ideally correspond to the pupillary and limbic boundaries, respectively.

In one hand, let $\mathcal{S}$ be a one-dimensional ordered set of sectors defined as the regions where the target boundary shape can reside at each given angular step. On the other hand, let $\mathcal{L}$ be a set of labels that incorporate the exhaustive collection of radii in which the limbic boundary can be found. This range is statistically constrained by physiological evidence. Hence, a labeling L assigns some radius label $L_r \in \{R_{min}, \ldots, R_{max}\}$ to each sector $s \in \mathcal{S}$. Then, the energy associated to a specific L is:

$$E(L) = \sum_{s \in \mathcal{S}} D_s(L_s) + \sum_{\{s,t\} \in \mathcal{N}} V_{s,t}(L_s, L_t), \tag{4}$$

where $D_s(\cdot)$ is the data penalty function, $V_{s,t}(\cdot)$ is the interaction potential or smoothing term, and $\mathcal{N}$ is the neighborhood set of all pairs of adjacent sectors. Hence, in this approach, the horizontal coherence of the target shape is constrained by a chainwise

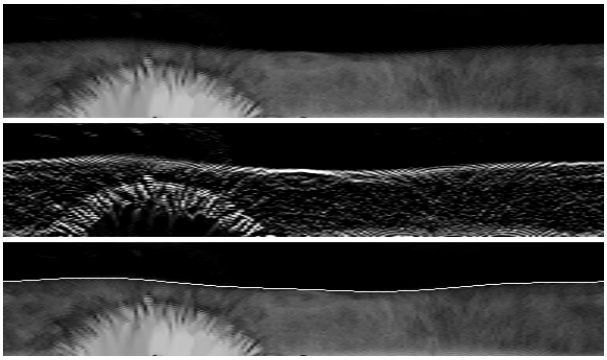

Fig. 4. Top down: original polar image of the pupil region after specularity removal, enhanced vertical gradient, and estimated pupillary boundary after graph cuts.

neighborhood, whereas the vertical coherence is achieved by imposing higher compatibility to closer radius labels, and lower compatibility to distant ones.

The data penalty term has been set to the vertical gradient of the polar image, which provides information about vertical discontinuities in the intensity map. Moreover, the interaction potential, which specifies the cost associated to changing the label of a sector from radius s to t, has been constructed by sampling a normal distribution centered at s along the whole range of possible radii, see Fig. 5. Thus, the sensitivity of the whole boundary localization process is controlled by a single parameter: the standard deviation σ of the normal distributions in the interaction potential, which influences the curvature of the resulting shape. The inference of the cut has average complexity of $O(|S| \log |S|)$.

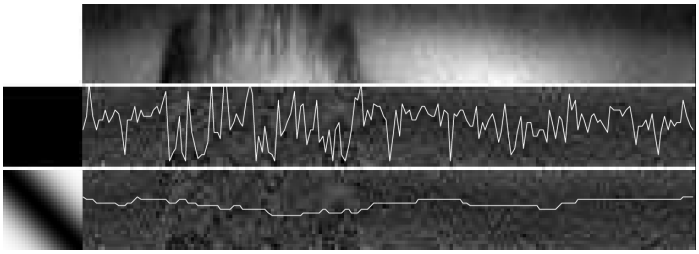

Fig. 5. Top down: original polar image (HID dataset) and minimal graph cuts for $\sigma = 400,8$ drawn over the computed gradient image. A visualization of the interlabel cost matrices (interaction potential) appears to the left of the gradient images.

3.4 Limbic boundary localization

Limbic boundaries are usually more challenging than pupillary ones, given the potential occlusions by the eyelids and eyelashes. However, this process can be eased by physiological evidence; as described in [4], the radius of the pupil varies within a range of 10–80% of the diameter of the iris. In addition, whereas it is common for the upper eyelid to notably overlap the iris region, the lower eyelid is usually less invading and presents minor to no overlapping.

Eyelid occlusion priors

In order to give more importance to those regions showing clear limbic boundaries, a probability function $pr(s)$ is estimated from over 1000 eyelid annotations done over samples from different databases. This function, shown in Fig. 6, gives information about the probability of not observing eyelid overlap at angle s, thus leaving out of the analysis those angular regions that are statistically prone to occlusions and artifacts.

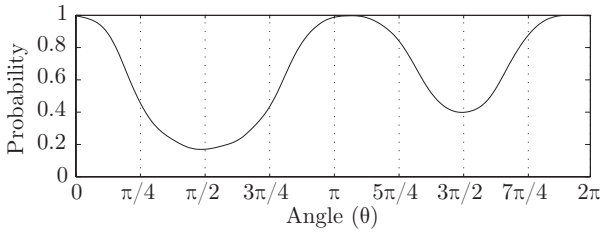

Fig. 6. Probability of not observing eyelid overlapping at angle θ. The upper eyelid corresponds to $\pi/2$, the lower one to $3\pi/2$.

Region bounding and contour fitting

A region of interest is placed at $[r-\Delta r, r+\Delta r]$ by maximizing Eq. (5) over the vertical gradient of polar image I.

$$\underset{r}{\operatorname{argmax}} \left| \int_{r-\Delta r}^{r+\Delta r} pr(s) \cdot \frac{\partial}{\partial r} I(s,r) dr \right| \tag{5}$$

Hence, contour fitting is then accomplished over this region by the graph cuts technique described for the pupillary boundary, see Fig. 5. Before applying graph cuts, some points are discarded if the local variance of each $r(s)$ is above a certain threshold, computed on a $[-L, L]$ neighborhood in Eq. (6).

$$\varepsilon(s) = \sum_{k=s-L}^{s+L} |r(k) - r(s)|^2 \tag{6}$$

4 Experimental validation

In order to conduct experimental validation of the presented segmentation algorithm, a new database identified as HID has been created, consisting of iris images captured under a series of unconstrained environments. These include different illumination conditions, variable distance ranges, presence of glasses and lenses, motion blur, and unfocused images, among others.

In addition, due to the lack of annotated iris segmentation resources, we have manually annotated two publicly available databases: MMU1[1] —450 irides— and IREX[2] —178 irides—, obtaining a final dataset of more than 1000 annotated irides. The HID iris database and the whole collection of annotations will be released to the research community. The performance of the presented method has been evaluated in terms of accuracy and speed. Two metrics have been considered: segmentation time and segmentation accuracy (SA) of the binary segmentation, defined as follows:

$$SA = \frac{TP}{TP + FP + FN} \tag{7}$$

being TP, FP, FN true positives, false positives and false negatives, respectively.

Table 1. Comparative results of traditional localization methods and our own over annotated databases. We show the results of the basic minimal cuts (MC) algorithm, as well as the contribution of eyelid priors (P).

Database		**Daugman**	**Wildes**	**MC**	**MC+P**
MMU1	**SA**	53.0 %	34.8 %	83.3 %	**84.0 %**
	Time	449 ms	196 ms	362 ms	**379 ms**
IREX	**SA**	77.9 %	72.8 %	79.5 %	**79.5 %**
	Time	1044 ms	816 ms	471 ms	**471 ms**
HID	**SA**	76.6 %	78.3 %	87.2 %	**88.3 %**
	Time	1132 ms	500 ms	397 ms	**385 ms**

Table 1 presents a comparison between our own method and the two most widely used algorithms for boundary localization, [3] and [12]. Given that Wildes and Daugman techniques require an exhaustive search that results in a very high computational cost, we first run our pupil localization method to reduce its search area to a region comprising the iris.

Our proposed method has been tested to assert the contribution of the two additional steps described, as can be seen in Fig. 7. Thus, two variation have been tested: the core

[1] http://pesona.mmu.edu.my/∼ccteo/

[2] NIST IREX III validation package from http://www.nist.gov/itl/ iad/ig/irexiii.cfm, which is a subset of the ND-IRIS-0405 dataset.

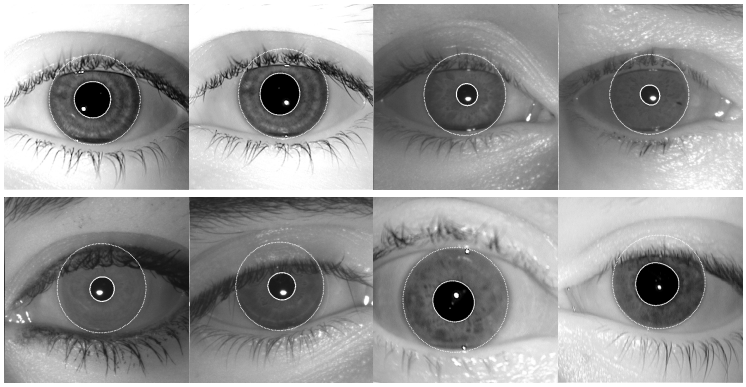

Fig. 7. Some examples of the success of our method. Sample images from different databases such as HID, ND-IRIS-0405, and MMU1.

minimal cut process (MC), and the cut with statistical eyelid priors (MC+P). All the experiments have been carried out on a 2.7 GHz dual-core machine with 4 GB of RAM, using non-optimized Matlab code.

5 Conclusions

In this work, an iris boundary localization method based on energy minimization by graph cuts is proposed, with previous preprocessing for coarse pupil localization and specular reflection removal. Recent advances on iris biometrics bring new challenges in terms of (i) robustness under unconstrained conditions and (ii) computational efficiency. These challenges are successfully addresses by the proposed novel method, which does not depend of rigid models, parameter sensitivity, and exhaustive searches. Furthermore, the solution can deal with iris low-constrained environments images. The evaluation has been carried out over three annotated public databases. Moreover, we have compiled our own dataset of low-constrained NIR iris images which will be released to the research community.

The localization of the limbic and pupillary boundaries is not the only problem of iris segmentation; subsequent processing includes upper and lower eyelid masking, eyelash segmentation, and localization of noisy regions such as shadows and corneal reflections, which will be addressed in our future work.

Acknowledgments

This work has been partially funded by the Spanish project SARAI (TEC2010–21040–C02–01). The authors would like to thank David Oro and Javier R. Saeta for their helpful discussions.

References

1. Y. Boykov and V. Kolmogorov. An experimental comparison of min-cut/max-flow algorithms for energy minimization in vision. *IEEE Trans. on Pattern Analysis and Machine Intelligence*, 26(9):1124–1137, 2004.
2. T. A. Camus and R. Wildes. Reliable and fast eye finding in close-up images. *International Conference on Pattern Recognition*, 1:389–394, 2002.
3. J. Daugman. High confidence visual recognition of persons by a test of statistical independence. *IEEE Trans. on Pattern Analysis and Machine Intelligence*, 15(11):1148–1161, 1993.
4. John Daugman. How iris recognition works. *IEEE Trans. on Circuits and Systems for Video Technology*, 14(1):21–30, 2004.
5. C. Fancourt, L. Bogoni, K. Hanna, Y. Guo, R. Wildes, N. Takahashi, and U. Jain. Iris recognition at a distance. In *Proc. IAPR Conf. Audio and Video Based Biometric Person Authentication*, pages 1–13. Springer, 2005.
6. Z. He, T. Tan, Z. Sun, and X. Qiu. Toward accurate and fast iris segmentation for iris biometrics. *IEEE Trans. on Pattern Analysis and Machine Intelligence*, pages 1670–1684, 2009.
7. P. Li, X. Liu, L. Xiao, and Q. Song. Robust and accurate iris segmentation in very noisy iris images. *Image and Vision Computing*, 28(2):246–253, 2010.
8. H. Proença and L. Alexandre. Ubiris: A noisy iris image database. *Image Analysis and Processing–ICIAP 2005*, pages 970–977, 2005.
9. SJ Pundlik, DL Woodard, and ST Birchfield. Non-ideal iris segmentation using graph cuts. In *Computer Vision and Pattern Recognition Workshops*. IEEE Computer Society, 2008.
10. T. Tan, Z. He, and Z. Sun. Efficient and robust segmentation of noisy iris images for non-cooperative iris recognition. *Image and Vision Computing*, 28(2):223–230, 2010.
11. M. Vatsa, R. Singh, and A. Noore. Improving iris recognition performance using segmentation, quality enhancement, match score fusion, and indexing. *IEEE Trans. on Systems, Man, and Cybernetics, Part B*, 38(4):1021–1035, 2008.
12. R. Wildes. Iris recognition: an emerging biometric technology. *Proceedings of the IEEE*, 85(9), 1997.